Ab Initio Study of the Hydrogen Bond and Proton Transfer in 2-(2′-Hydroxyphenyl)benzothiazole and 2-(2′-Hydroxyphenyl)bezimidazole

M. A. Ríos* and M. C. Ríos

Department of Physical Chemistry, Faculty of Chemistry, University of Santiago de Compostela, E-15706 Santiago de Compostela, Spain

Received: June 13, 1997; In Final Form: December 5, 1997

Ab initio HF/3-21G* and CIS/3-21G* calculations for the ground and the S_1 excited singlet states, respectively, of 2-(2′-hydroxyphenyl)benzothiazole (HBT) and 2-(2′-hydroxyphenyl)benzimidazole (HBI) were carried out. Geometric structures at the stationary points, including transition states, were investigated along with harmonic frequencies and hydrogen-bonding characteristics. A topological analysis of the density function, ρ, for the S_0 and S_1 states of the enol (N and N*) forms in the HBX series (X = −O−, −S−, and −NH−) provided some insight concerning the nature and trends of hydrogen bond interactions. The analysis of some parameters related to the intramolecular proton transfer suggests a qualitative relationship between the barrier height of the process and its exergonicity, consistent with principles of Leffler−Hammond and Bell−Evans−Polanyi and that changes in these two parameters are mainly determined by the strength of the hydrogen bond and to some extent by the electronegativity of X. Preliminary calculations carried out using continuum and specific models showed the important role of the specific effects of the solvent. Finally, some comments about dynamics were included.

Introduction

Proton transfer (PT) processes have for long aroused much interest in chemistry and biochemistry.[1−2] Also in recent years, intramolecular proton transfer has somehow been related to very important photophysical properties such as the laser dye activity[3−6] and polymer photostabilization[7−9] exhibited by some types of organic substances undergoing excited-state intramolecular proton transfer (ESIPT).[10−11] The chemical structure of these compounds usually contains a phenolic group which is intramolecularly hydrogen bonded to a heteroatom such as oxygen or nitrogen in the same chromophore; proton transfer takes place along the hydrogen bond.[12−14] 2-(2′-Hydroxyphenyl)benzoxazole (HBO),[15−20] 2-(2′-hydroxyphenyl)benzothiazole (HBT),[20,23−26] and 2-(2′-hydroxyphenyl)benzimidazole (HBI)[9,27−28] make up a compound series (HBX) that is representative of this structural frame, with −X− in the benzazole ring standing for −O−, −S− or −NH− (Figure 1). All these compounds undergo the chain of processes depicted in Figure 2 on excitation of the enol form (N).

Special attention has been paid to HBT, which can be taken as a reference for the other members in the series. Its rate of ESIPT is very high (about 6×10^{12} s^{-1} or 170 fs), which is attributed to motion along a low-frequency (100−300 cm^{-1}) coordinate rather than the high-frequency OH stretching mode, PT resulting from coupling between these two modes.[25,29−30] It is faster than vibrational and torsional relaxations ($k \approx 10^{11}$ s^{-1}) and exhibits no significant isotope effect,[31] which is suggestive of a barrierless process rather than tunneling. The estimated energy barrier for ESIPT is $\Delta H^{\ddagger} = 7$ kJ mol^{-1} and $\Delta H_0 = -38.5$ kJ mol^{-1},[32] the tunneling leading to an isotope effect that is probably undetectable under the experimental conditions. The resulting excited cis−keto tautomer, T*, is initially created with excess vibrational energy that is then dissipated on the 10−30 ps time scale[23−24,31] before Stokes-shifted fluorescence is emitted. Itoh et al.[33] calculated the rate of back PT in the ground state from T to N to be $k_{pT} = 5.8 \times 10^3$ s^{-1} with a kinetic isotope effect of 6.4. However, Brever et al.[34] proposed that the ground-state reverse PT takes place in less than 50 ns ($k_{pT} = 2 \times 10^{10}$ s^{-1}), which is much more consistent with other measurements of reverse PT than the rate reported by Itoh et al. This slow dynamics is assigned to a conformational change from the trans to the cis conformer.

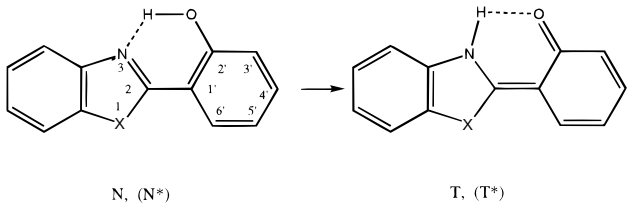

Figure 1. General structures for enol (N) and keto (T) forms of 2-(2′-hydroxyphenyl)benzazoles, HBX.

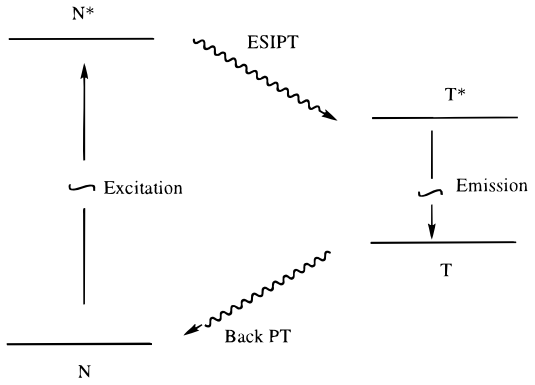

Figure 2. Chain of processes initiated by excitation of the enol forms (N).

The photophysics of HBO shares many characteristics with that of the related HBT. Most reported work on HBO only allowed the assignation of a lower limit about 10^{11} s^{-1} to the

S1089-5639(97)01949-X CCC: $15.00
Published on Web 02/10/1998

ESIPT rate constant.[16,35] Femtosecond pump−probe experiments carried out by Arthen-Engeland et al.[17] in cyclohexane at room temperature suggest an ESIPT time constant of 60 fs. As pointed out by Ormson and Brown,[11] this time constant cannot be regarded as defining the ESIPT rate constant since the rates of other processes could have been probed as well through the experiment undertaken by these authors.

The photophysics of HBI in solution conforms to a pattern similar to that for HBT and HBO, albeit with extremely high fluorescence yields.[36] This property has been shown to be a good basis for reasonably efficient laser action;[6] surprisingly, the benzimidazole system has attracted comparatively less interest.

In previous work,[22] we carried out ab initio calculations on HBO including partial exploration of the potential energy surfaces for states S_0 and S_1, calculations of energies and geometries at the stationary points, and the discussion of some dynamics-related aspects. As far as HBT and HBI are concerned, no experimental structural data other than the X-ray geometry for HBT[37] has been so far reported to the best of our knowledge, and only semiempirical calculations[9,20] have been done with the exception of one ab initio STO-3G computation for the ground state of the N form of HBT.[19]

Since proton transfer takes place along the hydrogen bond, a better understanding of the structural features of the bond and of its relationship to the transfer could shed some light on the underlying mechanism and the structural resources controlling such an important process. With this purpose, we carried out more rigorous and complete ab initio calculations on the N and T forms, as well as on the corresponding transition states (TS) for the ground and S_1 excited states of HBT and HBI, following the guidelines of our previous work on HBO. Also, we obtained specific results for the hydrogen bond, some of them drawn off in the frame of the theory of atoms in molecules,[38] and performed a general analysis for the HBX series of the relationships among hydrogen bond and selected parameters, some of them related to the intramolecular proton transfer. Furthermore, we carried out preliminary calculations of the effects of the solvent on some of the above mentioned parameters.

Calculations

Ab initio quantum chemical calculations were carried out within the limits of Born−Oppenheimer approximation. On the basis of the size of the HBX molecules, their ground and S_1 states were investigated at the SCF/3-21G* and CIS/3-21G* level, respectively. It seems to be well established[39−43] that inaccuracies due to the crudity of the 3-21G* basis and to the lack of correlation cancel each other out to a certain extent. According to Pople et al.,[44] "a satisfactory exploration of the potential energy surfaces and accurate electronic properties of excited states are possible by the use of CI-singles gradients". All geometrical optimizations were performed without constraints. All calculations were done by using the GAUSSIAN94[45] software package.

The theory of atoms in molecules[38] was used in a topological analysis of charge density ρ in order to predict some characteristics of the hydrogen bond. The interaction of two atoms leads to the formation of a bond critical point at $\mathbf{r}_c$ in the charge density, a point where

$$\nabla\rho(\mathbf{r}_c) = 0 \quad \text{and} \quad (\lambda_1 < 0, \lambda_2 < 0, \lambda_3 > 0) \qquad (1)$$

λ_1, λ_2, and λ_3 being the curvatures of ρ. This point is labeled $(3, -1)$ according to its rank and signature.[46] Vectors defining the axes of these principal curvatures bound the interatomic surface and bond path. The charge density is a maximum in the interatomic surface at $\mathbf{r}_c$ (λ_1 and λ_2, normal to the bond path, are negative) and charge is locally concentrated there. ρ is a local minimum at $\mathbf{r}_c$ along the bond path ($\lambda_3 > 0$), and charge is depleted there with respect to neighboring points along the bond path. Thus, an interatomic surface and a chemical bond are the result of a competition between the normal contractions of ρ toward and along the bond path and parallel expansion of ρ leading to the separate contraction of charge in the basins of the neighboring atoms. The sign of $\nabla^2(\rho)$ at $\mathbf{r}_c$ determines which of the two competing effects prevails. When $\nabla^2(\rho) < 0$, normal contractions in ρ predominate and electronic charge is shared among the nuclei as is typical for covalent bonds. When $\nabla^2(\rho) > 0$, the contraction of each atomic density toward its nucleus predominates and leads to charge depletion at $\mathbf{r}_c$, which is typical of the so-called "closed-shell interactions" observed in noble gas repulsive states, ionic bonds, and hydrogen bonds. The PROAIM software suite was used to perform the charge density analysis.[47]

Results and Discussion

Equilibrium Geometries. Although the subject of this work was the HBX series, only the results for HBT and HBI are explicitly included in this section as the geometry is concerned; those for HBO were reported in a previous paper.[22]

The fully optimized geometrical parameters for the N (a) and T (b) tautomers of HBT in the S_0 and S_1 states are shown in Figure 3a,b and those for HBI in Figure 4a,b. The eight structures were tested for the stationary point condition using frequency calculations.

The eight structures exhibit C_s symmetry; also excitation of the N forms causes geometrical changes that involve significant shifts toward keto forms, leading to N* structures more favorable for transfer.

A comparison of the results for the ground-state N form of HBT (Figure 3a) with those provided by X-ray measurements[37] reveals that the X-ray bond lengths for 2′−O, 3′−4′, and 5′−6′ are shorter whereas those for 1′−2′, 2−1′, and 2′−3′ are longer than the HF/3-21G* calculated values, that for 2−3 being almost identical to its calculated counterpart (Table 1). This suggests that hydroxyphenyl moiety of the HBT molecule in the crystal state is partly converted into a quinoid-like form, as previously pointed out by Enchev.[20] Despite these special features, there is acceptable agreement between the experimental and HF/3-21G* results; also the latter are slightly better than previously reported AM1[20] and HF/STO-3G[19] results, as shown by the root-mean-square values included in Table 1.

Hydrogen Bond. As stated in the Introduction, expanding available knowledge on the features of intramolecular bonding along the HBX series could provide a better understanding of the intramolecular proton transfer.

With this purpose, the HBX series was enlarged to include the case HBM, where X = $-CH_2-$ and the calculations were extended to the eight S_0 and S_1 open forms—those where the OH group is rotated by 180°. The differences in energy and some other parameters between H-bonded and nonbonded forms are given in Table 2. If these energy differences are taken to be estimates of the hydrogen bond energies, the strength of the hydrogen bond increases from the ground to the S_1 excited state and also along the HBX series in the following sequence: $-O- < -S- < -CH_2- < -NH-$ (the energies for $-S-$ and $-NH-$ are almost identical in the S_1 state). The net charges of the H and N atoms increase upon the hydrogen bonding

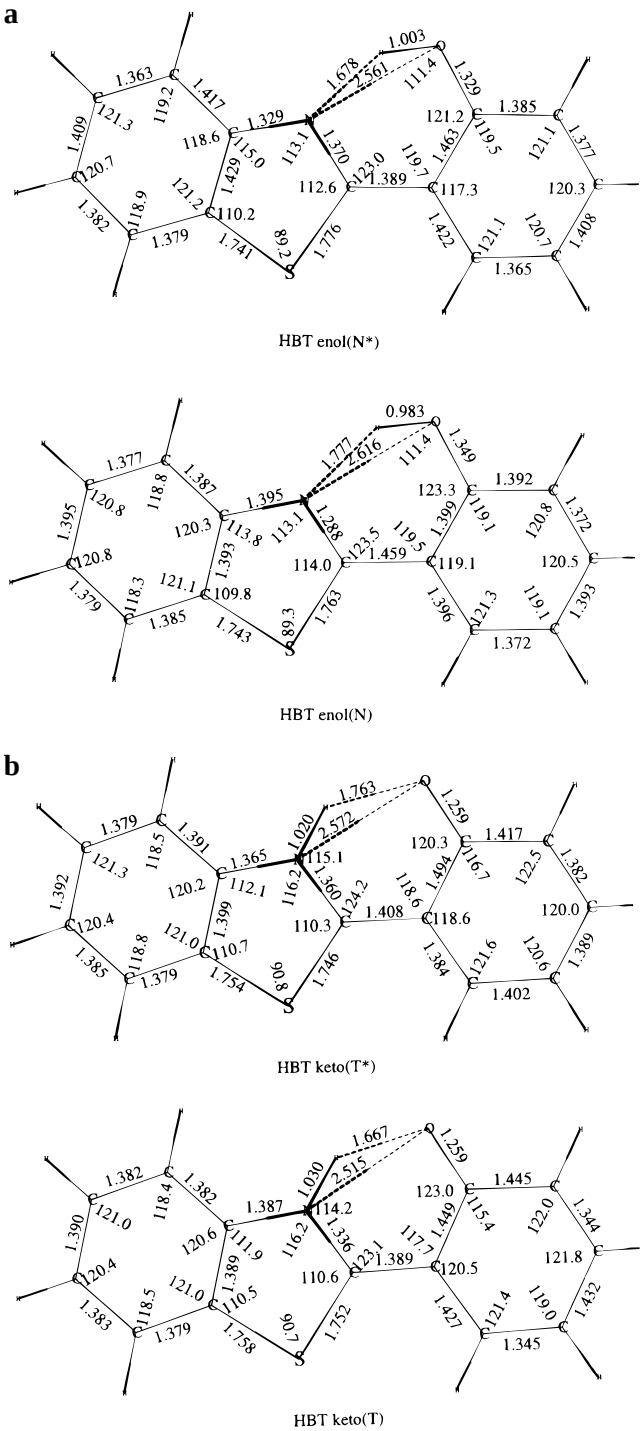

Figure 3. Geometrical parameters for HBT. (a, top) Enol in S_0 (N) and S_1 (N*) states. (b, bottom) Keto in S_0 (T) and S_1 (T*) states. Distances are in angstroms and angles in degrees.

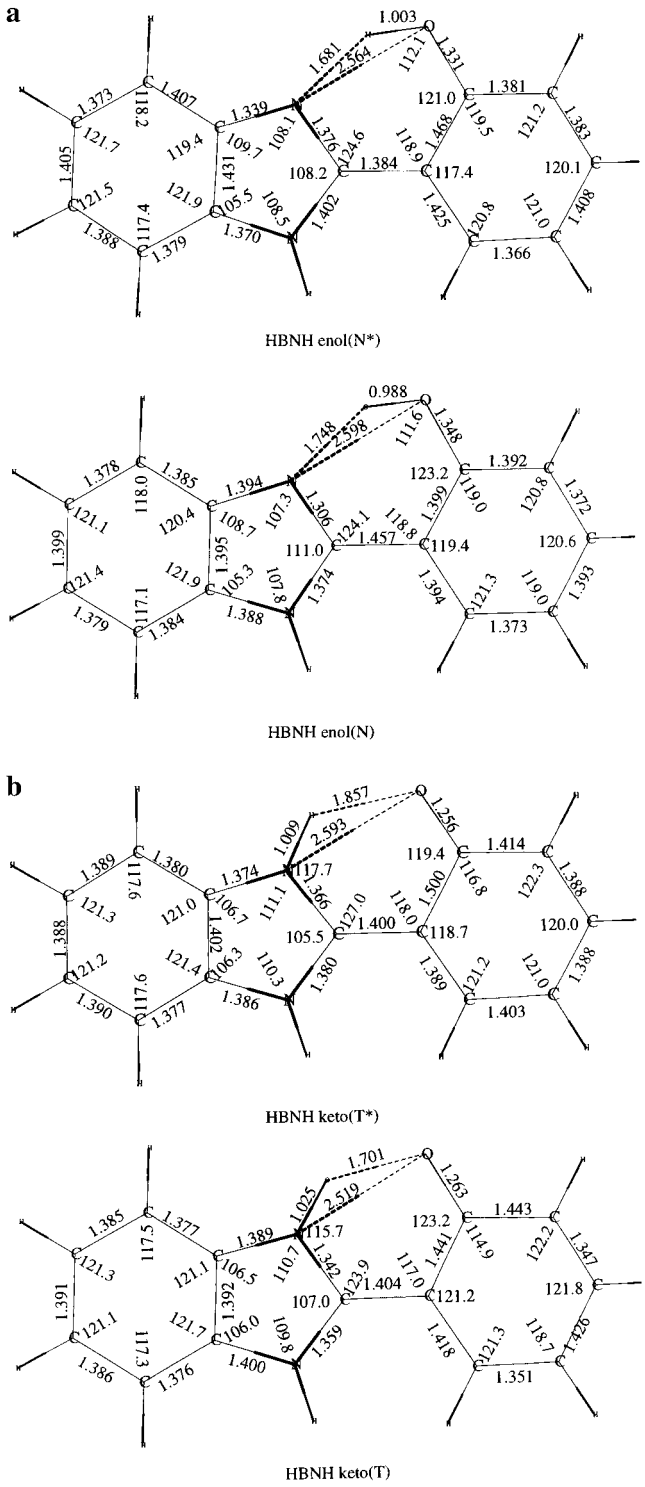

Figure 4. Geometrical parameters for HBI. (a, top) Enol in S_0 (N) and S_1 (N*) states. (b bottom) Keto in S_0 (T) and S_1 (T*) states. Distances are in angstroms and angles in degrees.

and are consistent with the assumed hydrogen bond strength. On the other hand the OH bond lengths increase on hydrogen bonding in the same sequence order as the energy does; by contrast, ν for OH stretching (in Table 4) and the d_{O---N} distances decrease in the same sequence. The "inherent" electronegativity of X for the valence states of the ground state $tr^2trtr\pi^2$ (for O and S), $trtrtr\pi^2$ (for N),[49] and tetete (for C) are also included in Table 2. The strength of the intramolecular hydrogen bond seems to be qualitatively related with the electronegativity of X (it decreases with increasing X electronegativity if the electronegativity prevails over the other factors) and also with the delocalization of the charge. The $-CH_2-$ group has a low electronegativity but it does not allow the delocalization. The results in Table 2 also show that, as a rule, the molecular framework around the hydrogen bond undergoes a significant rearrangement when the OH hydrogen is H-bonded by the N atom (O---N approach mutually as the chief result of the decreased 2−1′ bond length and 1−2−1′ and 2−1′−2′ bond angles). The low C−S−C bond angle in HBT results in a less marked effect.

In order to improve our understanding of the hydrogen bonding and transfer, we also carried out an analysis of the

TABLE 1: Experimental and Calculated Bond Lengths of HBT[a]

source	d(2′−O)	d(3′−4′)	d(5′−6′)	d(1′−2′)	d(2′−3′)	d(2−3)	d(2−1′)	RMS
AM1 (20)	1.366	1.383	1.384	1.409	1.416	1.227	1.453	0.036
HF/STO-3G (19)	1.373	1.374	1.375	1.409	1.406	1.306	1.489	0.025
HF/3-21G*	1.349	1.372	1.372	1.399	1.392	1.288	1.459	0.021
X-ray (37)	1.305	1.349	1.356	1.411	1.422	1.280	1.481	

[a] Distances in angstroms. RMS = root-mean-square deviations from the X-ray values of all the C−C, C−O, C−S, and C−N bond lengths

TABLE 2: Hydrogen Bond: Energy and Main Geometric and Charge Effects[a]

molecule	state	ΔE_H	Δd_{OH}	$\Delta d_{12'}$	$\Delta(\Sigma\theta)$	$\Delta d_{O\cdots N}$	Δq_H	Δq_N	χ(X)
HBO(N)	S_0	−58.6	+0.016	−0.013	−4.1	−0.133	+0.057	−0.141	16.7
HBT(N)	S_0	−69.1	+0.018	−0.011	−2.5	−0.094	+0.062	−0.159	10.9
HBI(N)	S_0	−78.5	+0.024	−0.011	−3.7	−0.130	+0.068	−0.164	9.6
HBM(N)	S_0	−72.7	+0.020	−0.092	−3.4	−0.102	+0.065	−0.166	7.4
HBO(N*)	S_1	−64.9	+0.031	−0.004	−6.8	−0.188	+0.069	−0.165	
HBT(N*)	S_1	−79.5	+0.038	−0.011	−5.3	−0.150	+0.075	−0.184	
HBI(N*)	S_1	−79.3	+0.038	−0.005	−5.6	−0.167	+0.078	−0.186	
HBM(N*)	S_1	−81.4	+0.034	−0.078	−4.5	−0.153	+0.077	−0.210	

[a] Δ = differences between H-bonded and open structures. $\Sigma\theta = \theta_{121'} + \theta_{212'} + \theta_{1'2'0}$. E in kJ mol^{-1}, d in angstroms, and θ in degrees. χ = inherent electronegativity, eV.

TABLE 3: Hydrogen Bond, Density Function[a]

molecule	state	ρ(N--H)	$\nabla^2\rho$(N--H)	r_H/r_N	$\Delta(r_H+r_N)$	ρ(OH)	$\nabla^2\rho$(OH)	ρ(ring)
HBO(N)	S_0	0.0401	0.117	0.527	1.617	0.309	−1.763	0.0168
HBT(N)	S_0	0.0474	0.124	0.510	1.743	0.306	−1.764	0.0179
HBI(N)	S_0	0.0500	0.125	0.502	1.800	0.300	−1.718	0.0179
HBO(N*)	S_1	0.0492	0.118	0.501	1.793	0.291	−1.619	0.0179
HBT(N*)	S_1	0.0585	0.122	0.479	1.930	0.283	−1.550	0.0187
HBI(N*)	S_1	0.0575	0.123	0.481	1.924	0.283	−1.547	0.0182

[a] r_i = distance from the bond critical point to the nucleus i. Δ = differences of $r_H + r_N$ with respect to the sum of the van der Waals radii. ρ, $\nabla^2\rho$, and Δr are in atomic units.

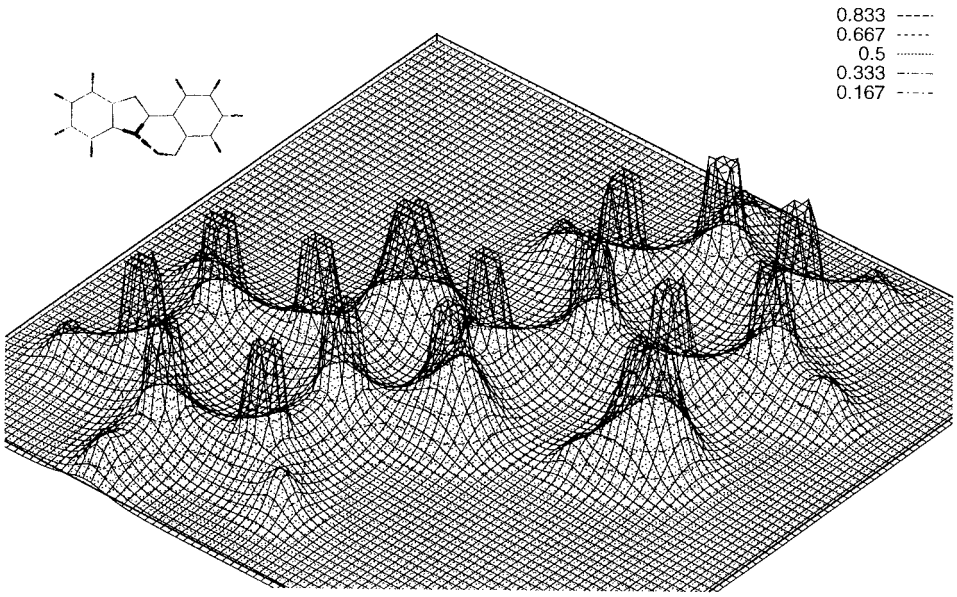

Figure 5. A contour map of the density function, ρ, for the N form of HBO in the S_0 state.

density function, ρ, in light of the theory of atoms in molecules. Bond critical points and ring points were calculated; the results for the hydrogen bond, OH bond, and −N--HOCCC− pseudoaromatic ring are given in Table 3. For OH bond critical points, $\rho(\mathbf{r}_c) \approx 0.30$ au and $\nabla^2\rho(\mathbf{r}_c) \approx -1.6$ au, consistent with a covalent interaction; for H---N hydrogen bonds, $\rho(\mathbf{r}_c) \approx 0.05$ au and $\nabla^2\rho(\mathbf{r}_c) \approx 0.12$ au. The latter values indicate the absence of charge concentration at $\mathbf{r}_c$ between H and N, shared by both atoms; rather, there is the depletion typical of closed-shell interactions. Charges concentrate in the basins of the atoms and can be polarized in the bonded region, thus giving rise to bound states. By way of example, Figure 5 presents ρ for the N form of HBO on a relative scale. Ring critical points (3, 1) have also been observed for the pseudoaromatic ring closed by the hydrogen bond. Upon hydrogen bonding, OH bonds are weakened and the systems stabilized through the pseudoaromatic rings. Density changes at the critical points are quite consistent with the aforementioned trends in ΔE_H and hence with the previously found relation between $\rho(\mathbf{r}_c)$ and hydrogen bond energies.[48] The $r_{N\cdots H}$ hydrogen bond distance is the sum of the bonded radii r_H and r_N—the distances from the bond critical point to the respective nuclei—and is compa-

TABLE 4: Selected Parameters Related to Proton Transfer[a]

molecule N, TS, T	ΔE N → T	$\Delta V^{\ddagger}$ N → T	$\Delta V^{\ddagger}$ N ← T	d_{OH} N	d_{O--H} TS	d_{O--H} T	d_{O--N} N	d_{O--N} TS	d_{H--N} N	ν(OH) N	ν(O--N) N
HBO(S_0)	+47.0	57.5	10.8	0.980	1.338	1.781	2.671	2.386	1.843	3601	125
HBT(S_0)	+42.5	49.4	6.8	0.983	1.328	1.667	2.616	2.388	1.777	3540	131
HBI(S_0)	+30.5	39.6	9.1	0.988	1.309	1.701	2.598	2.381	1.748	3430	137
HBO(S_1)	−30.2	15.5	45.9	0.996	1.189	1.893	2.616	2.408	1.751	3270	123
HBT(S_1)	−29.7	10.0	42.3	1.003	1.167	1.763	2.561	2.399	1.679	3115	128
HBI(S_1)	−41.8	9.5	51.1	1.003	1.165	1.857	2.564	2.404	1.681	3111	133

[a] ΔE and $\Delta V^{\ddagger}$ in kJ mol^{-1}; ν = unscaled values in cm^{-1}.

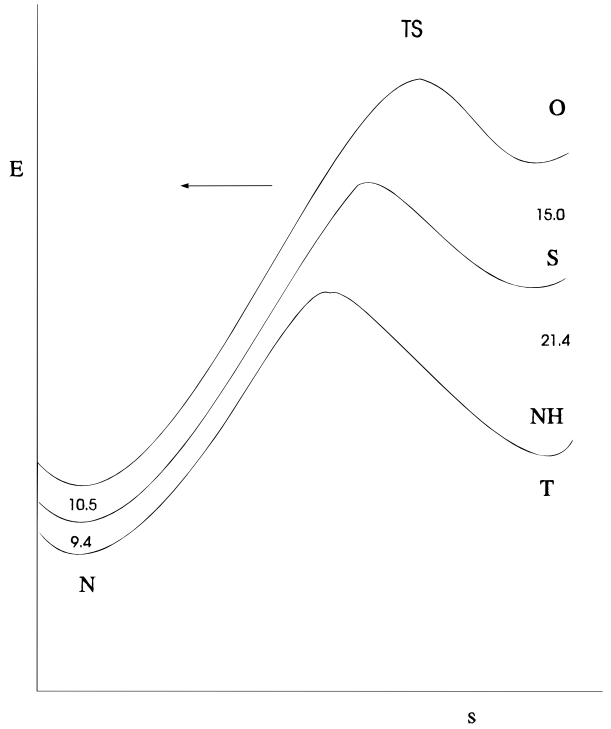

Figure 6. Effects of the X substitution on exergonicity (ΔE), position of the transition state, and barrier height for the process N → T in HBX series. (Values = energy differences in kJ m^{-1}; s = IRC).

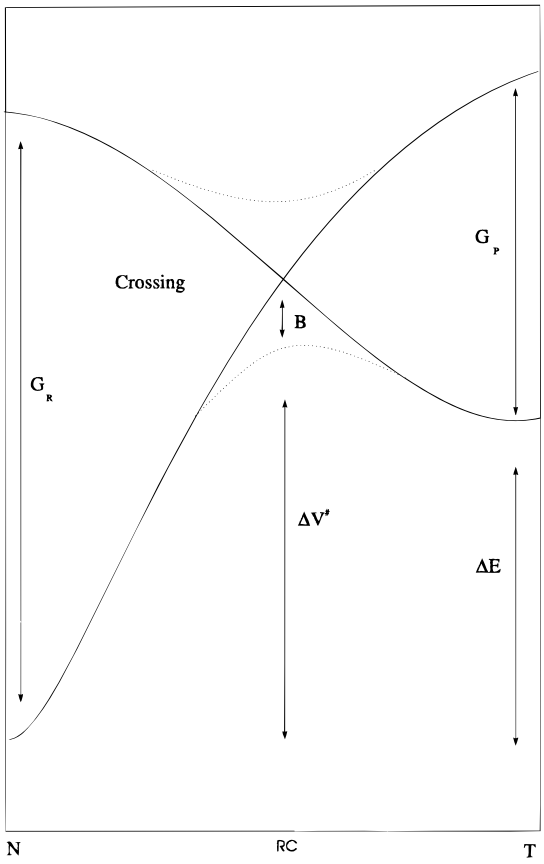

Figure 7. A general state correlation diagram for N → T processes in HBX series. (RC = reaction coordinate).

rable to the sum of the van der Waals radii (5.10 au). The differences, Δ, between r_{H---N} and this value, included in Table 3, provide a measure of the penetration undergone by the van der Waals envelopes of the H and N atoms upon the formation of the hydrogen bond and seem to correlate fairly well with the hydrogen bond energies listed in Table 2. On the basis of the r_H/r_N ratio, the bond critical point comes closer to H than to N as the hydrogen bond strength and charge of N increase.

Intramolecular Proton Transfer. Selected parameters related to proton transfer are collected in Table 4. All the members in the HBX series exhibit transition states that are product-like ("late") for endothermic processes in the ground state and reactant-like ("early") for exothermic processes in the S_1 excited state, as previously shown for HBO.[22]

X substitution increases exergonicity—the difference, ΔE, between the energies of the T and N forms—of the reaction, from −O− to −NH−. Because this substitution also stabilizes the N forms through an increased hydrogen bond energy, ΔE_H, T forms should be stabilized to a greater extent and lead to a situation similar to that depicted in Figure 6, viz. a shift in the transition state toward "early" positions along the reaction coordinate and a lower barrier. Both effects, which seem to be confirmed by the results of Table 4, are in agreement with the Leffler−Hammond postulate[50,51] and the Bell−Evans−Polanyi (BEP) principle.[52,53] According to Shaik et al.,[54] there is an approximate expression for the $\Delta V^{\ddagger} - \Delta E$ relation

$$\Delta V^{\ddagger} \approx \left\{ f_R + f_P + (1 - f_R - f_P)\frac{\Delta E}{G_R} \right\} \frac{G_R(G_P + \Delta E)}{G_R + G_P} \quad (2)$$

where, as illustrated in Figure 7, G_R and G_P are the energy gaps from singlet to triplet of the OH and NH bonds, f_R and f_P are related to the curvatures, and B is the degree of avoided crossing. The $\Delta V^{\ddagger} - \Delta E$ relation (the BEP principle) holds provided f, G, and B remain almost constant, which is likely to be the case because we are dealing with a series of reactants that only differ in the X substituent, which takes no direct part in the transfer. However, the very early position of the transition state in the S_1 excited state will result in a very large (and difficult to measure) rate constant for the ESIPT which can appear to be not very sensitive to the effects of the substituents.

On the basis of the data of Tables 2 and 4, the barrier height decreases with increasing hydrogen bond strength and decreasing electronegativity of X, consistent with the above considerations. The barrier height also seems to decrease with decreasing distance between O and N, the heavy atoms in the hydrogen

TABLE 5: Solvent Effects[a]

model		continuum(SCIPCM)				specific(H_2O)		dipole moment	
state		S_0				S_0	S_1	S_0	S_1
$\epsilon/n(H_2O)$		1	2.0	35.9	78.3	1	1		
HBO	ΔE	47.0	41.6	33.6	33.3	10.0	−78.3		
	$\Delta V^{\ddagger}_{N\rightarrow T}$	57.5	53.7	48.4	48.2			2.63	4.83
	$\Delta V^{\ddagger}_{T\rightarrow N}$	10.8	12.5	14.8	14.9				
HBT	ΔE	42.5	37.8	30.4	30.7	8.9	−60.3		
	$\Delta V^{\ddagger}_{N\rightarrow T}$	49.4	45.8	40.2	40.2			2.70	4.45
	$\Delta V^{\ddagger}_{T\rightarrow N}$	6.8	8.0	9.9	9.5				
HBI	ΔE	30.5	23.9	14.3	13.9	−11.6	−81.4		
	$\Delta V^{\ddagger}_{N\rightarrow T}$	39.6	34.8	27.7	27.4			4.39	6.20
	$\Delta V^{\ddagger}_{T\rightarrow N}$	9.1	10.9	13.4	13.6				

[a] ϵ = dielectric constant. n = number of water molecules. Energies in kJ mol^{-1}. μ = debye.

bond system. The ΔE and $\Delta V^{\ddagger}$ values calculated for the ESIPT process of HBT (−29.7 and 10.0 kJ mol^{-1}) are reasonably consistent with those reported by Chou et al.[32] (−38.5 and 7 kJ mol^{-1}, respectively).

The unscaled harmonic frequencies of some a′ normal modes of N and N* that might be involved in the transfer processes are also given in Table 4. The ν_{OH} frequencies clearly follow the patterns of the hydrogen bond energies, ΔE_H, along the series. The low-frequency mode (ν_{ON}) involves mainly bending of the skeleton of the ring closed by the hydrogen bond and seems to be coupled with the proton transfer.

The above gas-phase results suggest an in-plane ESIPT mechanism in which the initial bending of the skeleton favors the approach of the N and O atoms; subsequently, the intramolecular proton transfer takes place properly, in a second step. The barriers obtained for ESIPT at this level of calculation are low, and they could become even lower if correlation effects were included, so that no tunneling can be expected (the effective barriers for tunneling, obtained from the minimum energy path barriers after correcting them with zero-point energies, adopt no meaningful values). In this context and only as a preliminary attempt, we calculated the rate constant for ESIPT in HBO—where the barrier is not so low—using the TST approach. The rate constant increases with T, and the value we arrived at is 5.88×10^{11} s^{-1} at 298 K, which seems to be a low value for this temperature, but reasonable, according to the value of the barrier. To the best of our knowledge only a lower limit of 10^{11} s^{-1} has been established at 11 K, using matrix isolation fluorescence spectroscopy. Neither the simple TST approach nor the basic RRKM theory can be applied to ESIPT in HBT and HBI, which exhibit loose transition states with very low barriers and require specific variational treatments.

Solvent Effects. To account for solvent effects on the intramolecular proton transfer processes in HBX series, two kinds of calculations were carried out: self-consistent isodensity polarized continuum model (SCI-PCM) calculations, as implemented in GAUSSIAN94,[45] and optimizations of supermolecules made up adding one water molecule to the system in the region of the intramolecular hydrogen bond.

Since a previous test done on the N form of HBO using the SCI-PCM model revealed that a complete optimization of the solvated system caused nearly zero changes in the geometric parameters in relation to their gas-phase values, no geometric optimizations have been carried out with this model. We studied the effects of three solvents of increasing dielectric constant—hexane ($\epsilon = 2.0$), acetonitrile ($\epsilon = 35.9$), and water ($\epsilon = 78.3$)—on the N, T, and TS forms of HBX molecules in their ground state (no code was available for excited-state CIS calculations). The obtained results, included in Table 5, show that the T forms become more stabilized by the solvent than the N forms due to their bigger dipole moment, and therefore the exergonicity and the barrier height of the N → T process decreases up to a limiting value as the dielectric constant increases. A similar behavior can be expected for the excited state because the dipole moments of T* forms in the excited state also are bigger than those of the N* forms.

The effects of the specific solvation, as they are shown by the limited supermolecule calculations carried out, are also included in Table 5. In this case, only the enol and keto molecular forms in both the ground and the excited states were optimized without restrictions, with one molecule of water located so as to be able to be H-bonded to the >N---H---O− system. Three different kinds of positions, displayed in Figure 8, have been found for the water molecule. The first of them, (a), is adopted by the N form of HBO, where the intramolecular hydrogen bond is weaker; in this case the system changes from C_s to C_1 symmetry at the same time as the intramolecular H-bond is being replaced by intermolecular bonds. Nearly the same occurs in the second case, (b), which is adopted by the T and T* forms of HBO, HBT, and HBI. Finally, the third kind of position, (c), where the water molecule does not break the intramolecular hydrogen bond, corresponds to the N* form of HBO and the N and N* forms of HBT and HBI. It is likely other positions of the water molecule, similar to the point of view of the energy, will to be found, mainly of the kind (c). Nevertheless, that the specific effects of the solvent are very important—mainly if the solvent is able to be hydrogen-bonded—and they are not included in the continuum models, that they increase the exergonicity of the intramolecular proton transfer processes and lower their barrier heights, and that these effects depend on the strength of the intramolecular hydrogen bond are general conclusions supported by the above preliminary results. The mechanisms and characteristics of the proton transfer can be changed by the specific effects of the solvent, even in the ground state, so this problem deserves a more complete and careful study.

Concluding Remarks

The reported ah initio calculations further support the role of the hydrogen bond in proton-transfer processes and mechanisms. The best equilibrium geometries reported so far for the N, N*, T, and T* forms of HBT and HBI are given in this paper. The energy differences between H-bonded and open enol forms were calculated as an index measuring the energy of the hydrogen bond and were successfully correlated, in qualitative terms, with other related parameters. The topological analysis of the ρ function provides a model for hydrogen-bonding interactions and also for their changes along the HBX series,

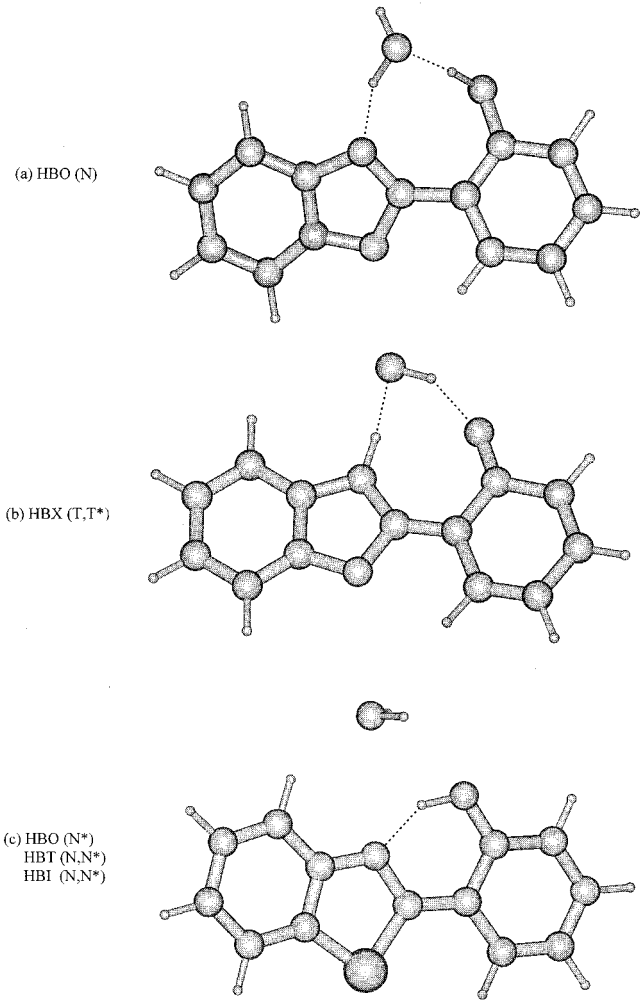

Figure 8. Specific solvation of HBX with one molecule of water. Different kinds of positions of the solvent molecule.

which seem to be determined to some extent by the electronegativity of X. In relation to the proton transfer in the gas phase, the results suggest an in-plane mechanism virtually identical with that proposed for HBO[22] where the transfer is coupled with some a′ low-frequency modes. The decrease in barrier height from the ground to the excited state and from −O− to −NH−, as well as the position of the TS, seem to be related to some extent to the strength of the hydrogen bond, consistent with the BEP principle and the Leffler−Hammond postulate. A very fast ESIPT that is difficult to measured can be expected from the very early positions of the TS and from the low barrier heights in the excited state. Preliminary calculations show that the solvent plays an important role in relation to the intramolecular proton-transfer processes and sometimes produces specific effects which can alter their mechanisms and characteristics.

Acknowledgment. We gratefully acknowledge generous allocation of time on the Fujitsu VP-2400 at the Centro de Supercomputacion de Galicia (CESGA) and on the Fujitsu VPP at the Computation Center of Nagoya University (Japan). This work was supported by the Ministerio de Educacion y Ciencia of Spain (Project PB94-0620). We also thank Prof. Bader for kindly providing us the PROAIM series of programs.

References and Notes

(1) Caldin, E. F., Gold, V., Eds. *Proton-Transfer Reactions*; Chapman and Hall: London, 1973.

(2) Arnaut, L. G.; Formosinho, S. J. *J. Photochem. Photobiol. A: Chem.* **1993**, *75*, 1.

(3) Chou, P. T.; McMorrow, D.; Aartsma, T. J.; Kasha, M. *J. Phys. Chem.* **1984**, *88*, 4596.

(4) Parthenopoulos, D. A.; McMorrow, D.; Kasha, M. *J. Phys. Chem.* **1991**, *95*, 2668.

(5) Acuña, A. U.; Costela, A.; Muñoz, J. M. *J. Phys. Chem.* **1986**, *90*, 2807.

(6) Acuña, A. U.; Amat, F.; Catalán, J.; Costela, A.; Figuera, J. M.; Muñoz, J. M. *Chem. Phys. Lett.* **1986**, *132*, 567. Costela, A.; Amat, F.; Catalán, J.; Douhal, A.; Figuera, J. M.; Muñoz, J. M.; Acuña, A. U. *Opt. Commun.* **1987**, *64*, 457. Costela, A.; Muñoz, J. M.; Douhal, A.; Figuera, J. M.; Acuña, A. U. *Appl. Phys. B* **1989**, *49*, 545.

(7) Durr, H.; Bouas-Laurent, H., Eds. *Photochroism. Molecules and Systems*; Elsevier: Amsterdam, 1990; Chapters 16 and 17.

(8) Rieker, J.; et al. *J. Phys. Chem.* **1992**, *96*, 10225.

(9) Catalan, J.; Fabero, F.; Guijarro, M. S.; Claramunt, R. M.; Santa-María, M. D.; Foces-Focess, M. C.; Hernández-Cano, F.; Elguero, J.; Sastre, R. *J. Am. Chem. Soc.* **1990**, *112*, 747.

(10) Formosinho, S. J.; Arnaut, L. G. *J. Photochem. Photobiol. A: Chem.* **1993**, *75*, 21.

(11) Ormson, S. M.; Brown, R. G. *Prog. React. Kinet.* **1994**, *19*, 45.

(12) Barbara, P. F.; Wals, P. K.; Brus, L. E. *J. Phys. Chem.* **1989**, *93*, 29.

(13) Rodríguez-Prieto, F.; Ríos, M. C.; Mosquera, M.; Ríos, M. A. *J. Phys. Chem.* **1994**, *98*, 8666.

(14) Mosquera, M.; Penedo, J. C.; Ríos. M. C.; Rodríguez-Prieto, F. *J. Phys. Chem.* **1996**, *100*, 5398.

(15) Williams, D. L.; Heller, A. *J. Phys. Chem.* **1970**, *74*, 4473.

(16) Woolfe, G. J.; Melzig, M.; Schneider, S.; Door, F. *Chem. Phys.* **1983**, *77*, 213.

(17) Arthen-Engeland, Th.; Bultman, T.; Ernsting, N. P.; Rodriguez, M. A.; Thiel, W. *Chem. Phys.* **1992**, *163*, 43.

(18) Lavtchieva, L.; Enchev, V.; Smedarchina, Z. *J. Phys. Chem.* **1993**, *97*, 306.

(19) Nagaoka, S.; Ithoh, A.; Mukai, K.; Nagashima, U. *J. Phys. Chem.* **1993**, *97*, 11385.

(20) Enchev, V. *Indian J. Chem.* **1994**, *33B*, 336.

(21) Das, K.; Sarkar, N.; Ghosh, A. K.; Majumdar, D.; Nath, D. N.; Bhattacharyya, K. *J. Phys. Chem.* **1994**, *98*, 9126.

(22) Ríos, M. A.; Ríos, M. C. *J. Phys. Chem.* **1995**, *99*, 12456.

(23) Barbara, P. F.; Brus, L. E.; Rentzepis, P. M. *J. Am. Chem. Soc.* **1980**, *102*, 5631.

(24) Ding, K.; Courtney, S. J.; Strandjord, A. J.; Friedrich, D.; Barbara, P. F. *J. Phys. Chem.* **1983**, *87*, 1184.

(25) Laermer, F.; Elsaesser, T.; Kaiser, W. *Chem. Phys. Lett.* **1988**, *148*, 119.

(26) Chou, P.; Martinez, M. L.; Studer, Sh. L. *Chem. Phys. Lett.* **1992**, *195*, 586.

(27) Das, K.; Sarkar, N.; Majumdar, D.; Bhattacharyya, K. *Chem. Phys. Lett.* **1992**, *198*, 443.

(28) Das, K.; Sarkar, N.; Ghosh, A. K.; Majumdar, D.; Nath, D. N.; Bhattacharyya, K. *J. Phys. Chem.* **1994**, *98*, 9126.

(29) Elsaesser, T.; Kaisser, W. *Chem. Phys. Lett.* **1986**, *128*, 231.

(30) Elsaesser, T.; Schmetzer, B.; Lipp, M.; Baeuerle, L. *J. Chem. Phys. Lett.* **1988**, *148*, 112.

(31) Barbara, P. F.; Rentzepis, P. M.; Brus, L. E. *J. Am. Chem. Soc.* **1980**, *102*, 2786.

(32) Chou, P. T.; Studer, S. L.; Martínez, M. L. *Chem. Phys. Lett.* **1991**, *178*, 393.

(33) Itoh, M.; Fujiwara, Y. *J. Am. Chem. Soc.* **1985**, *107*, 1561.

(34) Brewer, W. E.; Martínez, M. L.; Chou, P. T. *J. Phys. Chem.* **1990**, *94*, 1915.

(35) Mordzinski, A.; Grellmann, K. H. *J. Phys. Chem.* **1986**, *102*, 337.

(36) Sinha, H. K.; Dogra, S. K. *J. Chem. Phys.* **1986**, *90*, 5503.

(37) Stenson, P. *Acta Chem. Scand.* **1970**, *24*, 3729.

(38) Bader, R. F. W.; Nguyen-Dang, T. T. *Adv. Quantum Chem.* **1981**, *14*, 63. Bader, R. F. W.; Nguyen-Dang, T. T.; Tal, Y. *Rep. Prog. Phys.* **1981**, *44*, 893. Bader, R. F. W.; *Acc. Chem. Res.* **1985**, *9*, 18.

(39) Bicerano, J.; Schaefer, H. F., III; Miller, W. H. *J. Am. Chem. Soc.* **1983**, *105*, 2250.

(40) Frisch, M. J.; Scheiner, A. C.; Schaefer, H. F., III; Binkley, J. S. *J. Chem. Phys.* **1985**, *82*, 4194.

(41) Ríos, M. A.; Rodríguez, J. *J. Mol. Struct. (THEOCHEM)* **1991**, *228*, 149.

(42) Grana, A. M.; Ríos, M. A. *Struct. Chem.* **1991**, *2*, 575. Estévez, C. M.; Ríos, M. A.; Rodríguez, J. *Struct. Chem.* **1992**, *3*, 381.

(43) Ríos, M. A.; Rodríguez, J. *Can. J. Chem.* **1991**, *69*, 201; **1993**, *71*, 303.

(44) Foresman, J. B.; Head-Gordon, M.; Pople, J. A.; Frisch, M. J. *J. Phys. Chem.* **1992**, *96*, 135.

(45) Frisch, M. J.; Trucks, G. W.; Schlegel, H. B.; Gill, P. M. W.; Johnson, B. G.; Robb, M. A.; Cheeseman, J. R.; Keith, T. A.; Peterson, G.

A.; Montgomery, J. A.; Raghavachari, K.; Al-Laham, M. A.; Zakrzewski, V. G.; Ortiz, J. V.; Foresman, J. B.; Cioslowski, J.; Stefanov, B.; Nanayakkara, A.; Challacombe, M.; Peng, C. Y.; Ayala, P. Y.; Chen, W.; Wong, M. W.; Andrés, J. L.; Replogle, E. S.; Gomperts, R.; Martin, R. L.; Fox, D. J.; Binkley, J. D.; Defrees, D. J.; Baker, J.; Stewart, J. J. P.; Head-Gordon, M.; González, C.; Pople, J. A. GAUSSIAN94; Gaussian Inc.: Pittsburgh, PA, 1995.

(46) Carroll, M. T.; Chang, Ch.; Bader, R. F. W. *Mol. Phys*. **1988**, *63*, 387.

(47) Biegler-Konig, F. W.; Bader, R. F. W.; Tang, T. H. *J. Comp. Chem*. **1982**, *13*, 317.

(48) Boyd, R. J.; Choi, S. C. *Chem. Phys. Lett*. **1985**, *120*, 80; **1986**, *129*, 62.

(49) Hinze, J.; Jaffe, H. H. *J. Am. Chem. Soc*. **1962**, *84*, 540. Huheey, J. E. *J. Phys. Chem*. **1965**, *69*, 3284; **1966**, *70*, 2086.

(50) Leffler, J. E. *Science* **1953**, *117*, 340.

(51) Hammond, G. S. *J. Am. Chem. Soc*. **1955**, *77*, 334.

(52) Ogg, R. A.; Polanyi, M. *Trans. Faraday Soc*. **1935**, *31*, 604. Evans, A. G.; Evans, M. G. *Trans. Faraday Soc*. **1935**, *31*, 1401. Evans, M. G.; Polanyi, M. *Trans. Faraday Soc*. **1938**, *34*, 11. Evans, M. G.; Warhust, E. *Trans. Faraday Soc*. **1938**, *34*, 614.

(53) Bell, R. P. *Proc. R. Soc. London Ser. A* **1936**, *154*, 414. Bell, R. P.; Lidwell, O. M. *Proc. R. Soc London Ser. A* **1940**, *176*, 114. Bell, R. P. *J. Chem. Soc., Faraday Trans. 2* **1976**, *72*, 2088.

(54) Shaik, S. S.; Schlegel, H. B.; Wolfe, S. *Theoretical Aspects of Physical Organic Chemistry. The S_N2 Mechanism*; John Wiley & Sons, Inc.: New York, 1992.